Effect of mooring line attachment point on parametrically excited motions and power extraction in the Spar-buoy OWC device

Effect of mooring line attachment point on parametrically excited motions and power extraction in the Spar-buoy OWC device

G. Giorgi, G. Bracco &, G. Mattiazzo
Department of Mechanical and Aerospace Engineering (DIMEAS), Politecnico di Torino, Turin, Italy

R.P.F. Gomes
IDMEC, Instituto Superior Técnico, Universidade de Lisboa, Lisboa, Portugal

ABSTRACT: The Spar-buoy is an axisymmetric floating oscillating water column (OWC) wave energy converter. Minimizing the cost of energy requires an efficient power conversion while limiting costs and ensuring survivability. A critical and challenging design problem is the parsimonious definition of a compliant mooring system, assuring sea-keeping but with small impact on energy extraction. The mathematical model should be able to articulate parametric resonance (detrimental for power extraction and threatening survivability) and compute fast enough to extensively investigate the design space for the mooring layout optimization. Considering a three-line mooring system, alternative design solutions based on different fairlead attachment points are investigated with a computationally efficient nonlinear Froude-Krylov hydrodynamic model and a quasi-static inelastic line model. Results discuss the impact of mooring configurations on inducing parametric resonance (roll&pitch and yaw), on power extraction, and on the peak tension in the mooring lines. From the tested configurations, the most convenient appears to be with the attachment point close to the centre of gravity.

1 INTRODUCTION

Developers of wave energy converters (WECs) are striving for decreasing the cost of energy and become competitive in the renewable energy market. One major cost driver is the mooring system, which has the crucial role of assuring sea-keeping, both in operational and extreme conditions. However, oversizing for safety should be avoided, because the cost of the mooring lines usually amounts for a significant quota of the total structural expenditure (between 10% and 30%) (Xu et al., 2019). Moreover, a specific challenge of the WEC application case is that the mooring system should also be compliant with power absorption. Among several existing design solutions (Fitzgerald and Bergdahl, 2008), a popular configuration for floating WECs is with three lines equally spread around the device, with each line comprising of an anchor, a jumper (or riser), and a clump-weight (Pozzi et al., 2017). Such a system is ideal for WECs operating in pitch (Bracco et al., 2014; Pozzi et al., 2018) or heave (Correia da Fonseca et al., 2016), since it restrains surge with little impact on the degree of freedom (DoF) exploited for energy absorption. The relatively large pretension reduces the dynamic loads and the line shows good performance under extreme wave excitation (Moura Paredes et al., 2016).

The assessment of the performance of a mooring system is preferably performed experimentally (Sirigu et al., 2020; Moura Paredes et al., 2016) or with high-fidelity numerical models (Palm et al., 2016), because highly nonlinear extreme sea states are among the main barrage tests for accepting/refusing a specific mooring design candidate. However, assessing the impact on power conversion efficiency requires fast mathematical models, since a representative number of sea states should be investigated. Furthermore, optimizing the mooring configuration requires to explore a vast design space, so that a fast but also representative mathematical model should be considered.

On the one hand, there exist a large number of mathematical models for mooring systems (Davidson and Ringwood, 2017), filling the computation/fidelity continuum from quick quasi-static to accurate finite element methods. On the other hand, representative hydrodynamic models are often too slow to be used in optimization algorithms (Wendt et al., 2019). In particular, since floating WECs normally undergo large motions in order to maximize the extracted energy, nonlinear models may be required for reaching appropriate accuracy, especially when more then one degree of freedom (DoF) is considered (Novo et al., 2018; Giorgi and Ringwood, 2018a). Furthermore, the mooring system is particularly important when multi-DoFs systems are stud-

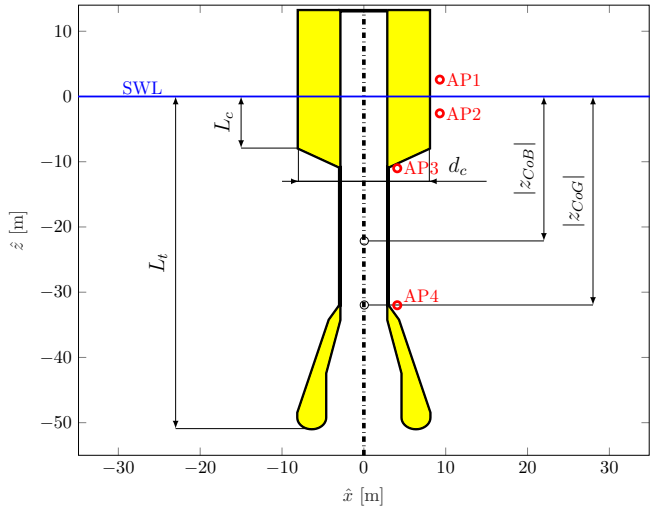

Figure 1: Section of the Spar-buoy OWC device. Important dimensions are tabulated in Table 2, where z_{CoG} is the centre of gravity and z_{CoB} is the centre of buoyancy. Four mooring line fairlead attachment points (AP) are represented.

ied, since they potentially provide restraint and coupling between all DoFs. In general, the design, optimization and assessment of a wave energy technology require detailed and representative mathematical models (Sirigu et al., 2020). Moreover, energy-maximizing controllers greatly benefit from the representativeness of such models (Bonfanti et al., 2018; Sirigu et al., 2019), due to their sensitivity to modelling error (Ringwood et al., 2018, 2019).

This paper focuses on the specific case of the Spar-buoy device, an axisymmetric floating oscillating water column (OWC), shown in Figure 1. This WEC generates energy from the air flow created by the relative motion between the floater and the water column within contained. This device is prone to experience parametric resonance, which is a highly-nonlinear phenomenon activated when the incoming wave has a period about half the natural period of the roll/pitch DoFs. As a result, despite of a planar 3-DoF external excitation, the floater develops a 5-DoF response due to internal parametric instability. Such a phenomenon is shown to be detrimental for power production (Gomes et al., 2020) and potentially threatening the device survivability (Giorgi and Ringwood, 2018b). However, (Correia da Fonseca et al., 2016) show experimentally that changing the mooring configuration can hinder the development of parametric response. Moreover, also the mooring system can induce parametric instability in the yaw DoF, as shown in (Orszaghova et al., 2020).

Although hydrodynamic parametric resonance of moored devices can be studied through fully-nonlinear models (Palm et al., 2018), it can also be articulated by nonlinear Froude-Krylov (NLFK) force models, which are based on linear-potential theory but consider the time-varying wetted surface to compute the exact Froude-Krylov (FK) force (Wang et al., 2019; Tarrant and Meskell, 2016). Traditional mesh-based approaches are computationally expensive, since they rely on a numerically discretized wetted surface that needs to be updated at each time step. However, for axisymmetric geometries there exist a computationally efficient approach that is able to compute in real time (Giorgi et al., 2020). Such a NLFK model is shown able to describe parametric instability for a simple spar-type device in regular (Giorgi and Ringwood, 2018d) and irregular waves (Giorgi and Ringwood, 2018c). An open-source demonstration toolbox is available (Giorgi, 2019), providing a ready-to-use implementation of the method.

Table 1: Dimensions (symbols defined in Figure 1) and inertial properties (mass (M) and inertias (I_x, I_y, and I_z)) of the floater.

Parameter		Value
d_c	[m]	16.00
L_c	[m]	7.91
L_t	[m]	50.91
z_{CoG}	[m]	-31.96
z_{CoB}	[m]	-22.14
M	[kg]	$2.86{\cdot}10^6$
$I_x = I_y$	[kg m^2]	$1.53{\cdot}10^9$
I_z	[kg m^2]	$1.12{\cdot}10^8$

This paper implements a 6-DoF NLFK approach to a 3-line moored Spar-buoy OWC device. The model, fully described in (Giorgi et al., 2020), comprising of computationally efficient NLFK force calculation and quasi-static model for the mooring system, is able to run in about real-time on a single processor of a conventional laptop. The objective is to investigate alternative design solutions based on different fairlead attachment points, studying the impact on both power conversion efficiency and parametric instability. The remainder of the paper is organized as follows: Sect. 2 briefly presents the characteristics of the device and its mathematical model, as well as the method of selection of the different mooring configurations considered in this work; Sect. 3 presents and discusses results; finally, Sect.4 provides final comments and concluding remarks.

2 SPAR-BUOY OWC DEVICE AND MATHEMATICAL MODEL

The Spar-buoy OWC device considered in this paper is the full-scale version of the prototype tested in the COAST laboratory ocean wave basin in Plymouth, UK (Correia da Fonseca et al., 2016). Important dimensions and inertial properties of the floater are tabulated in Table 2, whose geometrical symbols are defined in Figure 1.

The mooring system, schematically shown in Figure 2, is composed of three lines (diameter d_l, net density ρ_L^*) equally spaced in the radial direction around vertical axis of the buoy at rest. The anchors are placed on the sea floor, with water depth h, and at a radial distance R_a, relative to the buoy vertical axis

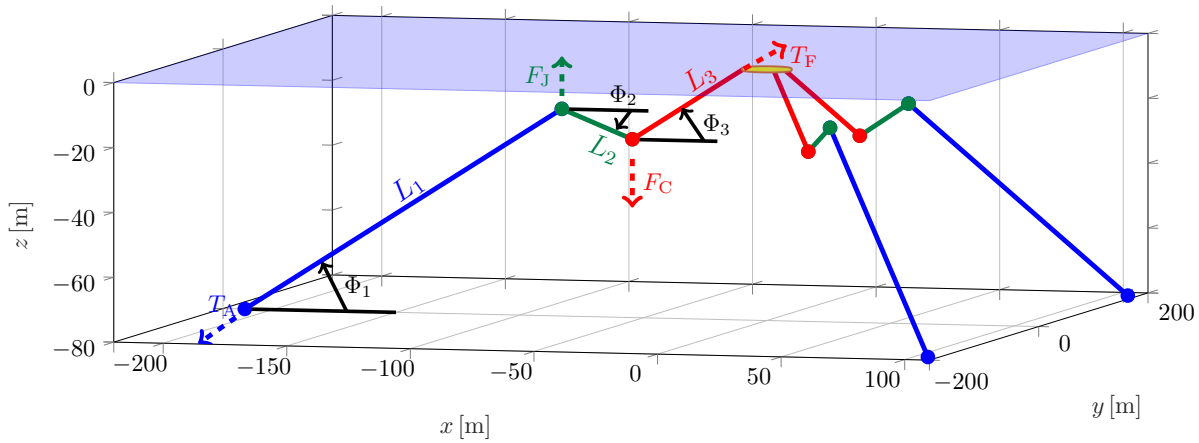

Figure 2: Mooring system layout with three lines 120° apart. Each line is divided in three segments of length L_1, L_2, and L_3. F_C is the net clump-weight force and F_J is the net jumper force. A quasi-static model solves for the tension at the vessel (T_v), the tension at the anchor (T_0), and the angles of the three lines (Φ_1, Φ_1, and Φ_3).

at rest. Each line is divided in ulterior three segments, connecting the anchor to a jumper (line of length L_1), then to a clump weight (line of length L_2), and finally to the buoy fairlead (line of length L_3). A quasi-static model is used to solve for the unknowns of the mooring system, defining a set of 5 nonlinear equations, shown in (1a)–(1e).

$$T_\mathrm{F} \sin\Phi_3 - T_\mathrm{A} \cos\Phi_1 - F_\mathrm{C} + F_\mathrm{J} + - w_\mathrm{L}\,(L_1 + L_2 + L_3) = 0 \tag{1a}$$

$$T_\mathrm{F} \cos\Phi_3 - T_\mathrm{A} \cos\Phi_1 = 0 \tag{1b}$$

$$T_\mathrm{F} \cos\Phi_3 z_\mathrm{F} - T_\mathrm{F} \sin\Phi_3 r_\mathrm{F} + F_\mathrm{C} r_\mathrm{C} - F_\mathrm{J} r_\mathrm{J} + + w_\mathrm{L}\,(L_1 r_1 + L_2 r_2 + L_3 r_3) = 0 \tag{1c}$$

$$L_1 \cos\Phi_1 + L_2 \cos\Phi_2 + L_3 \cos\Phi_3 - r_\mathrm{F} = 0 \tag{1d}$$

$$L_1 \sin\Phi_1 - L_2 \sin\Phi_2 + L_3 \sin\Phi_3 - z_\mathrm{F} = 0 \tag{1e}$$

where r_F and z_F are the horizontal and vertical distances between the buoy fairlead and the anchor, respectively, w_L represents the line submerged weight per unit length, and all other variables are defined in Figure 2.

While the density of the jumper (ρ_J) and of the clump-weight (ρ_C) are considered constant, their mass (M_J and M_C, respectively) is chosen according to the different mooring configuration. Alternative solutions are considered in this paper, namely changing the attachment point (AP) of the fairlead, as shown in Figure 1. One of the configurations tested in (Correia da Fonseca et al., 2016) is similar to AP2, which is therefore taken as a reference. Properties af AP2 are tabulated in Table 2. The turbine damping effect

Table 2: Properties of the mooring system AP2.

Parameter		Value
d_l	[mm]	32
ρ_L^*	[kg m^{-3}]	3.55
M_J	[kg]	4074
ρ_J	[kg m^{-3}]	123.00
M_C	[kg]	36300
ρ_C	[kg m^{-3}]	8097.50
L_1	[m]	143.28
L_2	[m]	37.01
L_3	[m]	50.40
R_a	[m]	211.2
h	[m]	80

is simulated by an equivalent orifice plate, whose diameter is optimized for each wave condition within a selection of 7 possible diameters.

This paper purports to investigate the influence of the attachment point on the device dynamics. However, for a fair comparison, all other relevant parameters should remain constant. Experiments in (Correia da Fonseca et al., 2016) show that the draft of the device has a great influence on parametrically excited motions. Similarly, (Giorgi et al., 2020) remarks the importance of the line pretension in modifying the response of the floater. Therefore, in this study, the mooring system parameters are chosen in order to obtain the same draft (L_c) and line pretension (T_{pre}) while changing the attachment point, as shown in Figure 1. The pretension is measured at the mooring segment attached to the buoy. The first point (AP1) is above the still water level, symmetric to AP2 relative to the water free surface; the third point (AP3) is at a lower level than AP2 and attached at a smaller radial distance from the axis; finally, AP4 is attached close to the centre of gravity. The roll/pitch restoring moment provided by the mooring lines greatly depends on the distance ($|\mathbf{r}_m - \mathbf{r}_g|$), where $\mathbf{r}_m$ is the position vector of the mooring attachment point and $\mathbf{r}_g$ is the position vector of the centre of gravity. More-

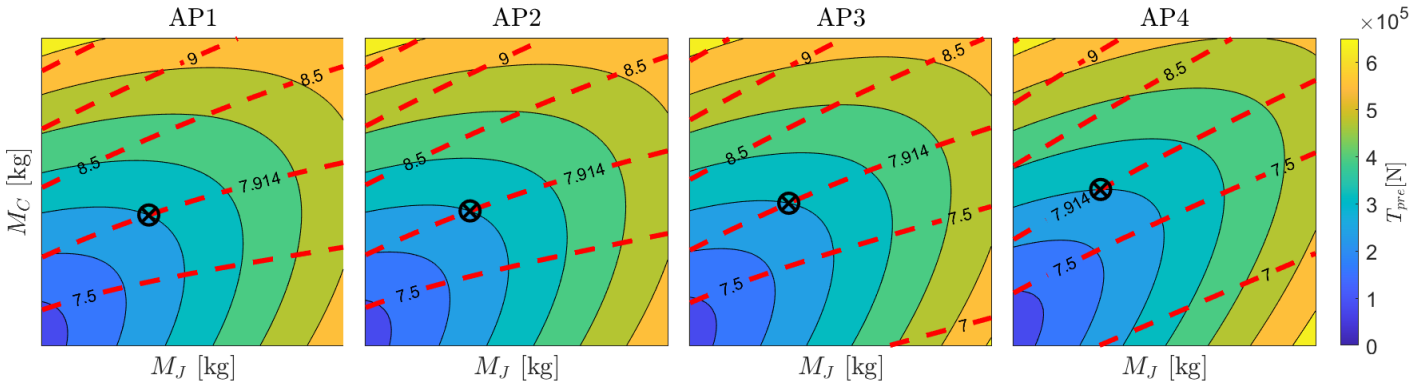

Figure 3: Maps of pretension (T_{pre}), with red-dashed-isolevels of the draft of the top cylinder (L_c), considering variations of jumper (M_J) and clump-weight (M_C) masses for each AP configuration. The identified pairs are shown by a marker, where $L_c = 7.914$m and $T_{pre} = 3.14 \cdot 10^5$N.

Table 3: Discriminating parameters across different mooring configurations.

		AP1	AP2	AP3	AP4
R_{AP}	[m]	9.28	9.28	4.08	4.08
z_{AP}	[m]	2.58	-2.58	-11	-32
$\lvert\mathbf{r}_m - \mathbf{r}_g\rvert$	[m]	35.77	30.81	21.35	4.08
α_L	[-]	0.88%	0%	0.95%	-1.68%
M_J	[kg]	4126	4074	3967	3730
M_C	[kg]	35500	36300	37800	40500

over, since the tension on the lines is highly sensitive to their length, a correction factor α_L is applied to each length (L_1, L_2, and $L3$), so that the length of line j of configuration k is computed as $L_{j,k} = L_{j,2}(1 + \alpha_L)$. The quantity $(1 + \alpha_L)$ is defined as the ratio between the distance from the anchor to the attachment point of configuration APj with respect to configuration AP2. Finally, Figure 3 shows the variations of T_{pre} and L_c for different jumper (M_J) and clump-weight (M_C) masses for each AP configuration. Such maps are used to identify the designed pairs of $L_c = 7.914$m and $T_{pre} = 3.14 \cdot 10^5$N. The parameters of each mooring configuration are detailed in Table 2.

2.1 *Nonlinear hydrodynamic model*

A time-domain nonlinear model is implemented to predict the response of the device for the four different mooring configurations. The model requirements are:

- Fast computation: many iterations are required to compute the response for a vast number of wave conditions, 7 control conditions, and 4 different mooring configurations.
- Ability to articulate parametric resonance: the objective of the study is to investigate the mutual dependence of the mooring system and parametric response.
- Include a fast model for predicting the mooring force.
- Include other relevant nonlienarities.

Therefore, a computationally efficient multi-DoF nonlinear Froude-Krylov force model is used, also including a quasi-static mooring model, nonlinear kinematics, centripetal and Coriolis effects, and viscous losses in all DoFs via integral representation. Seven DoFs are considered, 6 for the floater (x: surge, y: sway, z: heave, ϕ: roll, ϑ: pitch, and ψ: yaw), and the seventh for the inner water column elevation. A power take-off damping force, used for extracting energy, is modelled by means of an orifice plate, whose diameter is chosen among a selection of seven for each wave condition as the one that maximizes power production. Full details about the mathematical formulation are available in (Giorgi et al., 2020). Such a model is able to compute in real-time, i.e. the run time is about equal to the simulated time. An open-source demonstration toolbox implementing the computationally efficient NLFK force representation is provided in (Giorgi, 2019).

The mathematical model is used to estimate the natural periods in each DoF for the different mooring configuration, which are reported in Table 2.1. Heave, roll, pitch, and the water column are significantly insensitive to changes of attachment point, suggesting that power extraction capabilities are likely to remain similar. Moreover, the region of parametric instability also remains about constant, since it is located around $0.5T_{n,5}$. However, the width of the parametric resonance region and the intensity of parametric response cannot be inferred simply from the natural period analysis and need to be assessed through numerical simulation. Changes of natural period appear in surge and sway, decreasing as the attachment point sinks deeper. Conversely, a clear increase of the yaw natural period appears as the radial distance of the attachment point decreases, i.e. for AP3 and AP4. In fact, a smaller distance from the axis causes the yaw restoring torque to proportionally decrease and the natural period to increase.

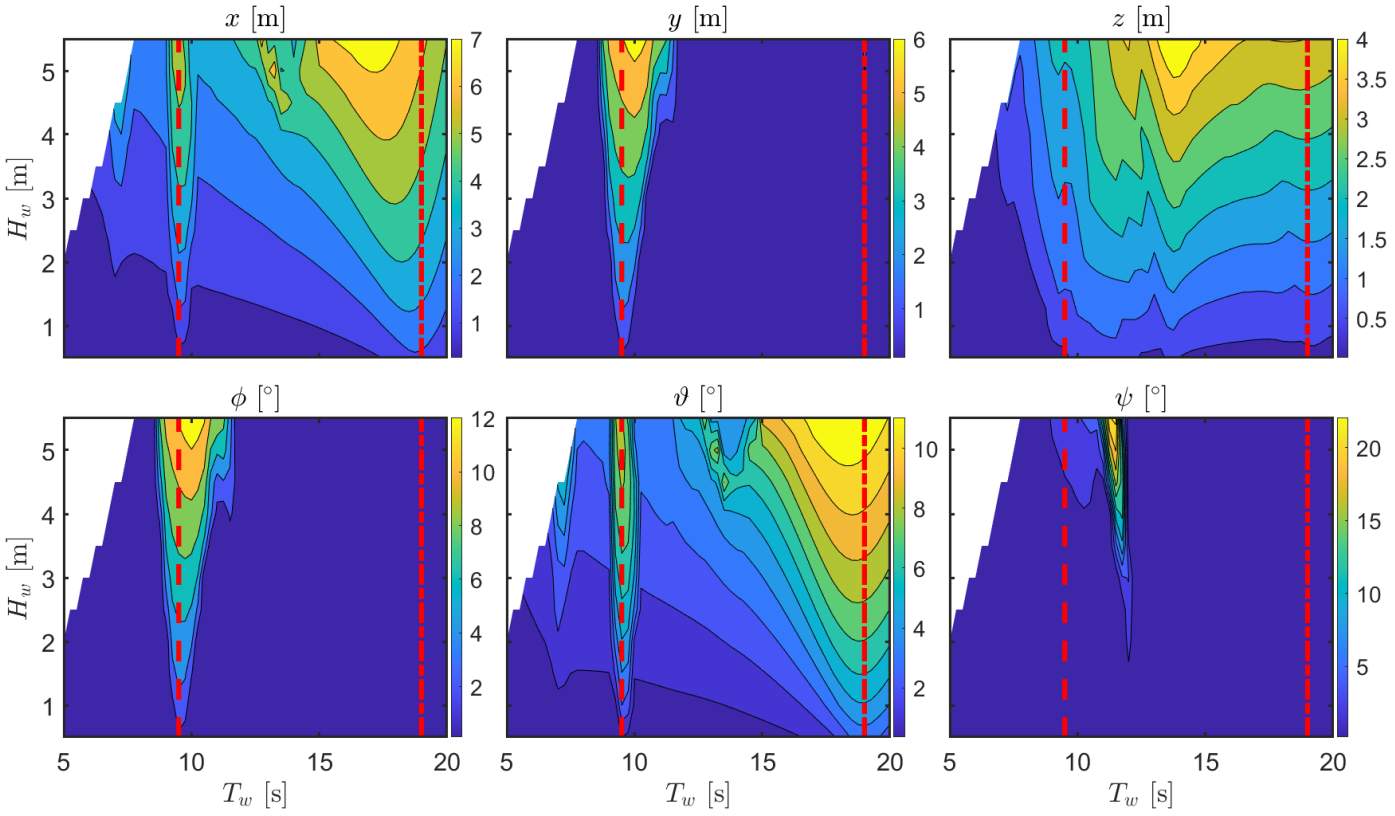

Figure 4: Amplitude of the response for configuration AP2 as a function of T_w and H_w. The dashed and dash-dotted red lines correspond to $T_w = \frac{1}{2}T_{n,5}$ and $T_w = T_{n,5}$, respectively.

Table 4: Natural periods in all degrees of freedom for the 4 different mooring configurations.

		AP1	AP2	AP3	AP4
$T_{n,1}$	[s]	152.4	149.0	136.3	126.2
$T_{n,2}$	[s]	152.8	149.4	137.1	127.7
$T_{n,3}$	[s]	10.3	10.3	10.3	10.3
$T_{n,4}$	[s]	18.9	19.0	19.3	19.2
$T_{n,5}$	[s]	19.1	19.1	19.3	19.2
$T_{n,6}$	[s]	24.1	24.1	36.9	36.8
$T_{n,7}$	[s]	13.7	13.7	13.7	13.7

3 RESULTS

A refined set of regular waves has been considered, propagating in the positive direction of x (see Fig. 2), with wave periods (T_w) from 5 s to 20 s, with step 0.25 s, and wave heights (H_w) from 0.5 m to 5.5 m, with step 0.5 m. However, the maximum wave steepness is limited to 6%. In fact, note that in Figure 4, as well as in all following contour plot figures, the top left corner presents no data, since those points realize a combination of T_w and H_w with a steepness higher than the 6% threshold. The effect of current has been neglected, since potential installation sites of the Spar-buoy device are characterized by low currents (Teillant et al., 2016). Figure 4 shows the amplitude of the response for configuration AP2, also highlighting where the wave period is $\frac{1}{2}T_{n,5}$ and $T_{n,5}$. The most remarkable result is the evident parametric resonance happening, as expected, at T_w around $\frac{1}{2}T_{n,5}$. Simulations show that the range of wave periods where the roll DoF is internally excited widens as the wave height increases, since greater incoming energy overcomes the internal damping more effectively. Since sway is coupled with roll, there is also a clear peak of the sway amplitude response across the same range of periods. Furthermore, note that also pitch engages into parametric resonance, since they have the same natural period due to the axisymmetric shape of the floater. Unlike roll, the range of wave periods in the pitch response with large amplitudes does not widens with the increase of H_w. It is likely that the external excitation of pitch due to wave action limits the level of energy capable of being absorbed by this mode, and in this case, the energy surplus is transferred to roll. Although the impact on the heave response is less evident, it can be noted that, when parametric resonance occurs, there is a drop in the heave amplitude, which is ultimately detrimental for power extraction. Finally, an isolated peak of yaw response can be found, suggesting that yaw can also be subject to a parametric-resonance-type effect due to the mooring system, similar to (Orszaghova et al., 2020).

The impact of different mooring configurations on power conversion efficiency is presented in Figure 5, showing significant insensitivity of the produced power. Note that there is a clear drop of absorbed power around the parametric resonance period ($T_w \approx \frac{1}{2}T_{n,5}$) region (red dashed line). Figure 6 considers the different roll, pitch, and yaw amplitudes for different mooring configurations. Moreover, an equivalent angle δ is defined in order to measure the overall

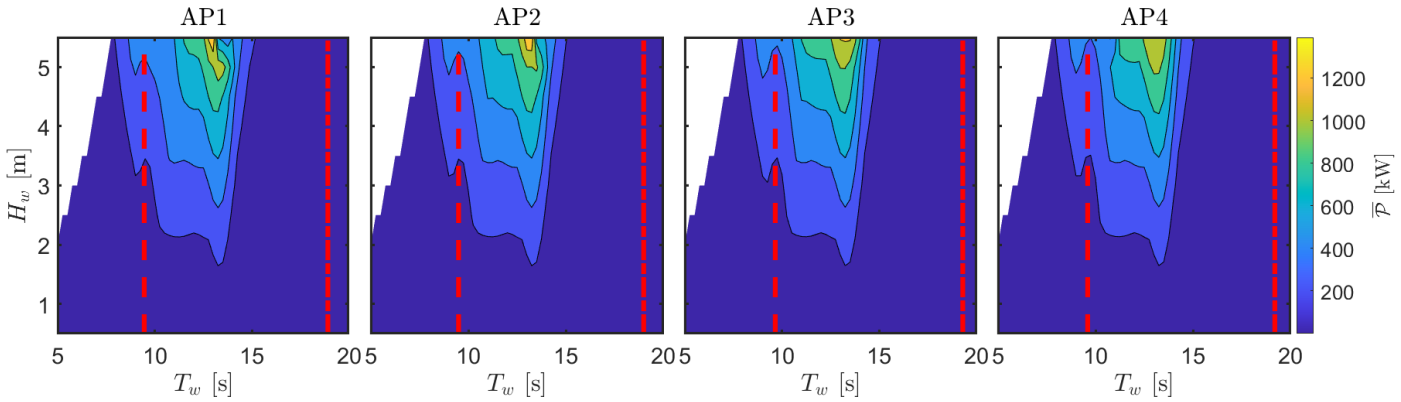

Figure 5: Produced power as a function of the wave period T_w and wave height H_w, for different mooring configurations. The dashed and dash-dotted red lines correspond to $T_w = \frac{1}{2}T_{n,5}$ and $T_w = T_{n,5}$, respectively.

multi-DoF rotation:

$$\delta(t) = \max \left| \angle \lambda \left(R_\psi R_\vartheta R_\psi \right) \right| \tag{2}$$

where λ computes the eigenvalues of the complete rotation matrix, obtained as the product of the single rotations matrix for yaw, pitch, and roll, according to the 3-2-1 convention (Giorgi et al., 2020). The last row of Figure 6 shows the mean of $\delta(t)$ as a metric for the maximum rotation amplitude.

The roll response (first row in Figure 6) shows a general decrease in both severity and width of the parametric resonance region as the attachment point moves deeper along the buoy. This suggests that the higher restoring torque due to a longer distance from the centre of gravity may contribute to feed energy into the generation of parametric instability, once this is triggered. However, such phenomenon is weak, since differences across mooring configurations are small. Conversely, the pitch response (second row in Figure 6) shows a slight increase for deeper AP. This may still be due to the lower restoring force that allows the external excitation to drive the floater further away from equilibrium. The yaw response (third row in Figure 6), which is not externally excited, still shows a response due to parametric excitation of the mooring system. Furthermore, the smaller distance of the attachment point from the axis, hence the smaller yaw stiffness, makes the severity of the yaw response significantly larger in AP3 and AP4. Finally, the mean equivalent maximum rotation angle (last row in Figure 6) shows that the highest values are obtained for AP1 and AP3. However, while the peak in AP1 is mainly due to the roll response, the peak in AP3 is due to the large yaw response.

Apart from the dynamic response of the floater, one major criterion that drives the design of a mooring system, therefore the choice of one configuration, is the maximum tension it has to withstand both during normal operation and extreme conditions. This paper considers regular waves that cover both operational and survivability regions, although extreme conditions are likely to appear in panchromatic waves due to constructive interference between frequency components. However, the qualitative and quantitative indications from regular waves can give meaningful characterization of the mooring configuration behaviour. Therefore, Figure 7 shows the maximum mooring tension (T_m), happening in the segment attached to the buoy of the front mooring line facing the incoming wave, for the different mooring configurations, with the color bar corresponding to the wave height. Note that all configurations have the same pretension, since this parameter was fixed in the design, as shown in Figure 3. The acceptability of the tensions reported in Figure 7 depends on the tensile properties of the mooring lines, which should be appropriately selected. Curves going beyond the limit of the vertical axis represent instances when the line becomes fully stretched, with all the three segments aligned. The only configuration that does not incur in these extreme loads is AP4. Furthermore, AP4 presents overall lower tensions across all investigated wave conditions. This is probably due to the reduced distance between the attachment point and the centre of gravity, as shown in Table 2.

4 CONCLUSIONS

The design of a compliant and cost-effective mooring system for wave energy converters is a challenging task, requiring representative and fast mathematical models. In the specific case of the Spar-buoy OWC device, parametrically excited motions are difficult to model and can affect both power conversion efficiency and mooring loads. However, appropriate design of the mooring system can help to counteract the development of parametric instability and decrease structural loads. This paper shows how a nonlinear Froude-Krylov force modelling approach is able to articulate parametric resonance in a computationally efficient way, making an extensive investigation of different mooring solutions in a wide range of wave conditions. However, such a method can be simply applied to any axisymmetric floater and assist a vast variety of applications, including optimization,

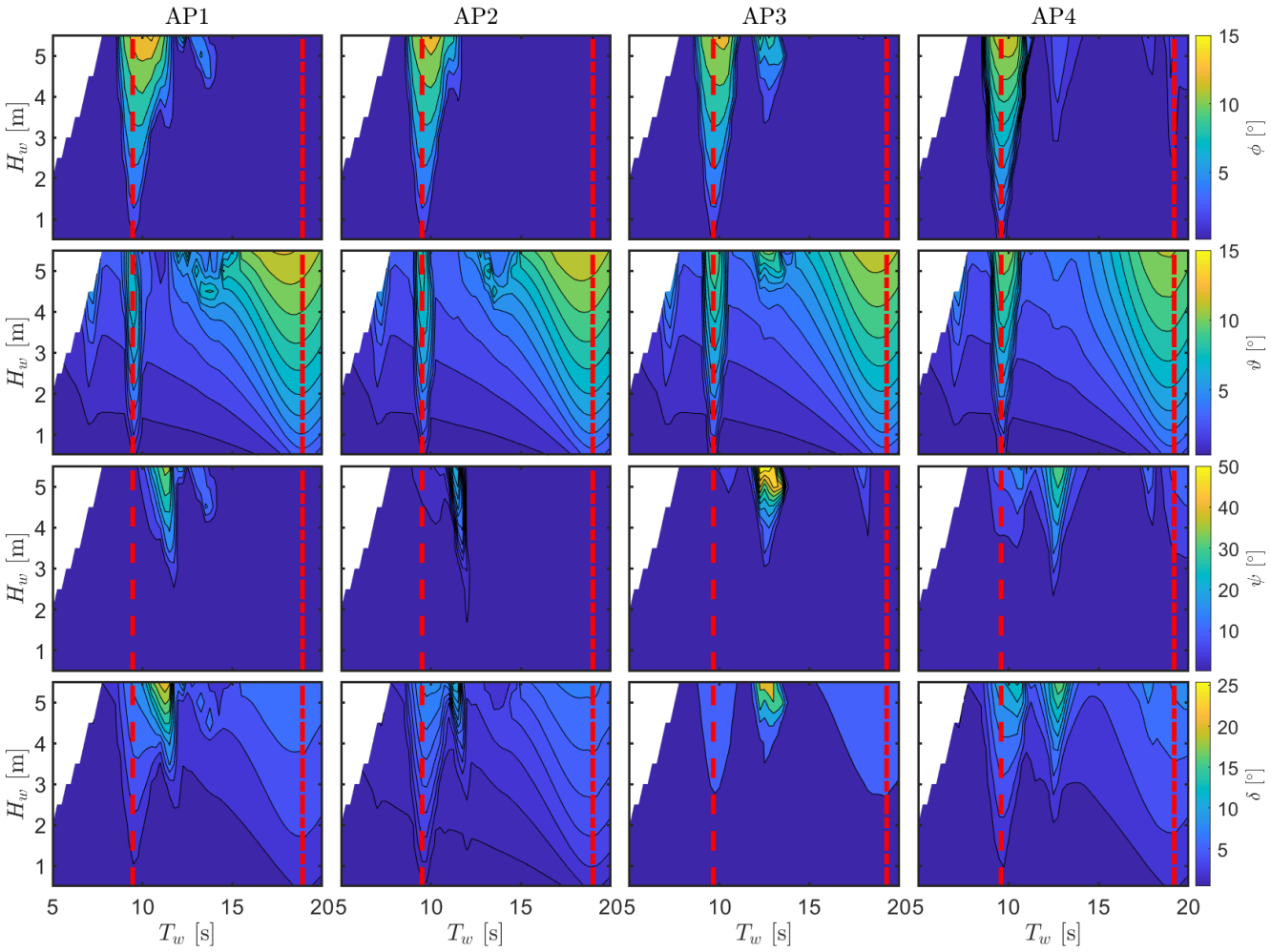

Figure 6: Amplitude of roll (first row), pitch (second row), yaw (third row) response. The forth row represents the mean maximum equivalent rotation, as defined in (2). The dashed and dash-dotted red lines correspond to $T_w = \frac{1}{2}T_{n,5}$ and $T_w = T_{n,5}$, respectively.

power conversion assessment, identification and control, thanks to real-time computation.

In this paper, the focus is on evaluating alternative design solutions based on the position of the attachment point of the fairlead of each mooring line. In particular, the impact on parametrically excited motions and power extraction is of interest. Results show that power conversion efficiency is significantly insensitive to the attachment point. However, the design solution with a deeper attachment point close to the centre of gravity seems to be more convenient because it results in lower overall rotations, lower parametric resonance and, most importantly, lower mooring tension and absence of events where the line becomes fully stretched. Furthermore, its mooring lines are shorter, hence less expensive. Finally, this study shows the potential development of yaw response induced by a parametric excitation of the mooring system. Such a response is influenced by the radial distance of the attachment point from the axis of the floater.

ACKNOWLEDGEMENTS

This research has received funding from the European Research Council (ERC) under the European Unions Horizon 2020 research and innovation program under Grant No. 832140. Computational resources provided by hpc@polito (http://hpc.polito.it)

REFERENCES

Bonfanti, M., G. Bracco, P. Dafnakis, E. Giorcelli, B. Passione, N. Pozzi, S. Sirigu, & G. Mattiazzo (2018). Application of a passive control technique to the ISWEC: Experimental tests on a 1:8 test rig. In *NAV International Conference on Ship and Shipping Research*, Number 221499, pp. 60–70.

Bracco, G., M. Casassa, E. Giorcelli, G. Giorgi, M. Martini, G. Mattiazzo, B. Passione, M. Raffero, & G. Vissio (2014). Application of sub-optimal control techniques to a gyroscopic Wave Energy Converter. In *Renewable Energies Offshore*, pp. 265–269.

Correia da Fonseca, F. X., R. P. Gomes, J. C. Henriques, L. M. Gato, & A. F. Falcão (2016). Model testing of an oscillating water column spar-buoy wave energy converter isolated and in array: Motions and mooring forces. *Energy 112*, 1207–1218.

Davidson, J. & J. V. Ringwood (2017). Mathematical modelling of mooring systems for wave energy converters - A review. *Energies 10*(5).

Fitzgerald, J. & L. Bergdahl (2008). Including moorings in the assessment of a generic offshore wave energy converter: A frequency domain approach. *Marine Structures 21*(1), 23–46.

Giorgi, G. (2019). Nonlinear Froude-Krylov Matlab demonstration toolbox.

Giorgi, G., R. P. F. Gomes, G. Bracco, & G. Mattiazzo (2020,

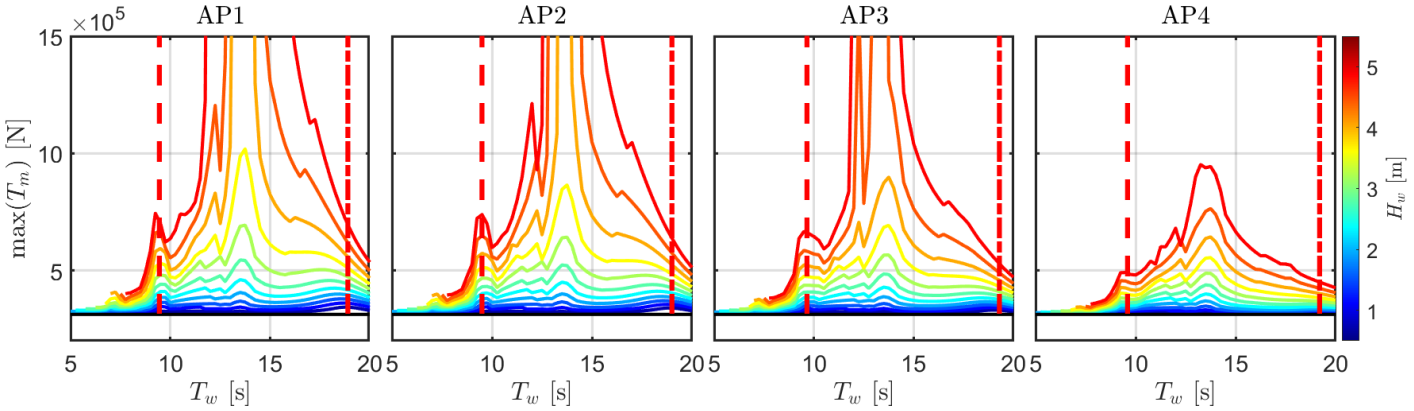

Figure 7: Maximum mooring line tension. The dashed and dash-dotted red lines correspond to $T_w = \frac{1}{2}T_{n,5}$ and $T_w = T_{n,5}$, respectively.

jan). The Effect of Mooring Line Parameters in Inducing Parametric Resonance on the Spar-Buoy Oscillating Water Column Wave Energy Converter. *Journal of Marine Science and Engineering 8*(1), 29.

Giorgi, G. & J. V. Ringwood (2018a). Analytical Formulation of Nonlinear Froude-Krylov Forces for Surging-Heaving-Pitching Point Absorbers. In *ASME 2018 37th International Conference on Ocean, Offshore and Arctic Engineering*, Madrid.

Giorgi, G. & J. V. Ringwood (2018b). Articulating Parametric Nonlinearities in Computationally Efficient Hydrodynamic Models. In *Proceedings of the 11th IFAC Conferecne on Control Applications in Marine Systems, Robotics, and Vehicles*, Opatija.

Giorgi, G. & J. V. Ringwood (2018c). Articulating parametric resonance for an OWC spar buoy in regular and irregular waves. *Journal of Ocean Engineering and Marine Energy 4*(4), 311–322.

Giorgi, G. & J. V. Ringwood (2018d). Parametric motion detection for an oscillating water column spar buoy. In *Proceedings of the 3rd International Conference on Renewable Energies Offshore RENEW*, Lisbon.

Gomes, R. P. F., J. C. C. Henriques, L. M. C. Gato, & A. F. O. Falcão (2020, apr). Time-domain simulation of a slack-moored floating oscillating water column and validation with physical model tests. *Renewable Energy 149*, 165–180.

Moura Paredes, G., J. Palm, C. Eskilsson, L. Bergdahl, F. Taveira-Pinto, G. M. Paredes, J. Palm, C. Eskilsson, L. Bergdahl, & F. Taveira-Pinto (2016, sep). Experimental investigation of mooring configurations for wave energy converters. *International Journal of Marine Energy 15*, 56–67.

Novo, R., G. Bracco, S. Sirigu, G. Mattiazzo, A. Merigaud, & J. Ringwood (2018). Non-linear simulation of a wave energy converter with multiple degrees of freedom using a harmonic balance method. In *Proceedings of the International Conference on Offshore Mechanics and Arctic Engineering - OMAE*, Volume 10.

Orszaghova, J., H. Wolgamot, S. Draper, P. H. Taylor, & A. Rafiee (2020). Onset and limiting amplitude of yaw instability of a submerged three-tethered buoy. *Proceedings of the Royal Society A: Mathematical, Physical and Engineering Sciences*.

Palm, J., L. Bergdahl, & C. Eskilsson (2018). Parametric excitation of moored wave energy converters using viscous and non-viscous CFD simulations. In *Renew*, Number October.

Palm, J., C. Eskilsson, G. M. Paredes, & L. Bergdahl (2016). Coupled mooring analysis for floating wave energy converters using CFD: Formulation and validation. *International Journal of Marine Energy 16*, 83–99.

Pozzi, N., A. Bonetto, M. Bonfanti, G. Bracco, P. Dafnakis, E. Giorcelli, B. Passione, S. Sirigu, & G. Mattiazzo (2018). PeWEC: Preliminary design of a full-scale plant for the mediterranean sea. In *NAV International Conference on Ship and Shipping Research*, Number 221499, pp. 504–514.

Pozzi, N., G. Bracco, B. Passione, A. Sirigu Sergej, G. Vissio, G. Mattiazzo, & G. Sannino (2017). Wave Tank Testing of a Pendulum Wave Energy Converter 1:12 Scale Model. *International Journal of Applied Mechanics 9*(2).

Ringwood, J. V., A. Merigaud, N. Faedo, & F. Fusco (2018). Wave Energy Control Systems: Robustness Issues. In *Proceedinds of the IFAC Conference on control Aplications in Marine Systems, Robotics, and Vehicles*.

Ringwood, J. V., A. Merigaud, N. Faedo, & F. Fusco (2019, apr). An Analytical and Numerical Sensitivity and Robustness Analysis of Wave Energy Control Systems. *IEEE Transactions on Control Systems Technology*, 1–12.

Sirigu, A. S., F. Gallizio, G. Giorgi, M. Bonfanti, G. Bracco, & G. Mattiazzo (2020). Numerical and Experimental Identification of the Aerodynamic Power Losses of the ISWEC. *Journal of Marine Science and Engineering 8*(49), 1–25.

Sirigu, S., M. Bonfanti, P. Dafnakis, G. Bracco, G. Mattiazzo, & S. Brizzolara (2019). Pitch Resonance Tuning Tanks: A novel technology for more efficient wave energy harvesting. In *OCEANS 2018 MTS/IEEE Charleston, OCEAN 2018*.

Sirigu, S. A., M. Bonfanti, E. Begovic, C. Bertorello, P. Dafnakis, G. Bracco, & G. Mattiazzo (2020). Experimental Investigation of Mooring System on a Wave Energy Converter in Operating and Extreme Wave Conditions. *Journal of Marine Science and Engineering 8*(180), 1–31.

Tarrant, K. R. & C. Meskell (2016). Investigation on parametrically excited motions of point absorbers in regular waves. *Ocean Engineering 111*, 67–81.

Teillant, B., Y. Debruyne, A. Sarmento, T. Simas, M. Silva, R. Gomes, J. Henriques, M. Philippe, A. Combourieu, & M. Fontana (2016). D2.1 - Designs and specifications of an OWC able to integrate the negative spring. Technical report.

Wang, H., A. Somayajula, J. Falzarano, & Z. Xie (2019, dec). Development of a Blended Time-Domain Program for Predicting the Motions of a Wave Energy Structure. *Journal of Marine Science and Engineering 8*(1), 1.

Wendt, F., K. Nielsen, Y.-h. Yu, H. Bingham, C. Eskilsson, B. Kramer, A. Babarit, T. Bunnik, R. Costello, S. Crowley, G. Giorgi, S. Giorgi, S. Girardin, & D. Greaves (2019). Ocean Energy Systems Wave Energy Modeling Task : Modeling , Verification , and Validation of Wave Energy Converters. *Journal of Marine Science and Engineering 7*(379), 1–22.

Xu, S., S. Wang, & C. Guedes Soares (2019). Review of mooring design for floating wave energy converters. *Renewable and Sustainable Energy Reviews 111*(March), 595–621.